Earth Syst. Sci. Data, 6, 353–366, 2014
www.earth-syst-sci-data.net/6/353/2014/
doi:10.5194/essd-6-353-2014

Open Access Earth System Science Data

A high-frequency atmospheric and seawater pCO_2 data set from 14 open-ocean sites using a moored autonomous system

A. J. Sutton[1,2], C. L. Sabine[2], S. Maenner-Jones[2], N. Lawrence-Slavas[2], C. Meinig[2], R. A. Feely[2], J. T. Mathis[2], S. Musielewicz[1,2], R. Bott[2], P. D. McLain[2], H. J. Fought[3], and A. Kozyr[4]

[1]Joint Institute for the Study of the Atmosphere and Ocean, University of Washington, Seattle, Washington, USA
[2]Pacific Marine Environmental Laboratory, National Oceanic and Atmospheric Administration, Seattle, Washington, USA
[3]Battelle Memorial Institute, Columbus, Ohio, USA
[4]Carbon Dioxide Information Analysis Center, Oak Ridge National Laboratory, Department of Energy, Oak Ridge, Tennessee, USA

Correspondence to: A. J. Sutton (adrienne.sutton@noaa.gov)

Received: 6 May 2014 – Published in Earth Syst. Sci. Data Discuss.: 26 May 2014
Revised: 1 October 2014 – Accepted: 3 October 2014 – Published: 6 November 2014

Abstract. In an intensifying effort to track ocean change and distinguish between natural and anthropogenic drivers, sustained ocean time series measurements are becoming increasingly important. Advancements in the ocean carbon observation network over the last decade, such as the development and deployment of Moored Autonomous pCO_2 ($MAPCO_2$) systems, have dramatically improved our ability to characterize ocean climate, sea–air gas exchange, and biogeochemical processes. The $MAPCO_2$ system provides high-resolution data that can measure interannual, seasonal, and sub-seasonal dynamics and constrain the impact of short-term biogeochemical variability on carbon dioxide (CO_2) flux. Overall uncertainty of the $MAPCO_2$ using in situ calibrations with certified gas standards and post-deployment standard operating procedures is < 2 µatm for seawater partial pressure of CO_2 (pCO_2) and < 1 µatm for air pCO_2. The $MAPCO_2$ maintains this level of uncertainty for over 400 days of autonomous operation. $MAPCO_2$ measurements are consistent with shipboard seawater pCO_2 measurements and GLOBALVIEW-CO2 boundary layer atmospheric values. Here we provide an open-ocean $MAPCO_2$ data set including over 100 000 individual atmospheric and seawater pCO_2 measurements on 14 surface buoys from 2004 through 2011 and a description of the methods and data quality control involved. The climate-quality data provided by the $MAPCO_2$ have allowed for the establishment of open-ocean observatories to track surface ocean pCO_2 changes around the globe. Data are available at doi:10.3334/CDIAC/OTG.TSM_NDP092 and http://cdiac.ornl.gov/oceans/Moorings/ndp092.

1 Introduction

The global ocean as well as its interactions with the atmosphere, climate, and marine ecosystem is undergoing a rapid and dramatic transition as it responds to multiple drivers on timescales from days to decades. Sustained observations guide our understanding of this ever-evolving earth system, which, in turn, informs the development of solutions for human societies to cope with global change. The iconic Mauna Loa atmospheric carbon dioxide (CO_2) time series, or "Keeling curve", is an example of how observations gain importance with time, as they provide the basis for understanding future changes to the earth system in the context of current and historical observations (Keeling et al., 1976; Thoning et al., 1989; Hofmann et al., 2009). Similar "ocean observatories" must be sustained in order to track ocean

carbon uptake and ocean acidification in the midst of the large natural temporal and spatial variability in the marine environment. These observations will provide a record of past and current behavior of the ocean carbon system and are central to predicting its future.

While high-quality ocean carbon measurements collected on global hydrographic surveys have been carried out approximately once a decade since the 1980s, the scientific community identified that constraining ocean biogeochemical models would require much greater temporal and spatial resolution of field data (Sabine et al., 2010). Autonomous technology to measure surface ocean carbon was developed to address this need and has undergone rapid advancement in the last three decades (Takahashi, 1961; Weiss et al., 1982; Wanninkhof and Thoning, 1993; Feely et al., 1998; Pierrot et al., 2009). Autonomous underway systems that can measure the partial pressure of CO_2 (pCO_2) on ships were the first major breakthrough in our ability to collect high-frequency observations in the global ocean. These systems are designed to produce climate-quality data sets with measurements accurate to within 1 µatm for atmospheric CO_2 and 2 µatm for surface seawater pCO_2. This level of accuracy has allowed the scientific community to constrain regional sea–air CO_2 fluxes to 0.2 Pg C yr^{-1}, a level of resolution necessary to test process-based models and predict the future behavior of the carbon cycle (Bender et al., 2002; Pierrot et al., 2009).

While underway pCO_2 observations have greatly enhanced our understanding of the spatial variability in sea–air CO_2 fluxes (Takahashi et al., 2009; Wanninkhof et al., 2013), they have not solved the problem of quantifying temporal variability at a given point in space. In highly variable regions such as the equatorial Pacific and coastal systems, fixed, high-frequency observations can improve our understanding of how short-term variability impacts CO_2 flux. Episodic phenomena are important drivers of biogeochemical variability, and mooring time series of pCO_2 and related properties provide the ability to assess the controls and impacts at these short timescales. Seawater pCO_2 observations that fully capture diurnal variations at a fixed site can also be used to test parameterizations of carbon cycle processes used in ocean biogeochemical models. The Moored Autonomous pCO_2 ($MAPCO_2$) system was developed to address this need by autonomously measuring surface ocean pCO_2 and marine boundary layer (MBL) atmospheric CO_2 every 3 h on surface buoys at approximately the same level of accuracy as underway pCO_2 systems. With this recent development of mooring autonomous pCO_2 technology, the combination of all three monitoring approaches (i.e., hydrographic surveys, underway, and buoy measurements) has improved our understanding of the spatial and temporal variability of ocean carbon at the sea surface. For the first time, ocean pCO_2 observations from multiple platforms have been incorporated into the most recent update (v2.0) of the Surface Ocean CO_2 Atlas (SOCAT), a data synthesis effort aimed at bringing together all available CO_2 data in the surface ocean in a common format (Bakker et al., 2014). The data presented here are identical to those in SOCATv2.0.

Here we describe the methods, data quality control (QC), and data access for an open-ocean $MAPCO_2$ data set collected on 14 surface buoys from 2004 through 2011. These surface ocean pCO_2 observatories are critical for characterizing the natural variability of the ocean carbon cycle, contributing to our understanding of secular trends in ocean chemistry, validating and interpreting modeling results, and developing more sophisticated global carbon models.

2 Methods and data quality control

In 2004, the National Oceanographic and Atmospheric Administration's (NOAA) Pacific Marine Environmental Laboratory (PMEL) began to work with the Monterey Bay Aquarium Research Institute to improve the accuracy, reliability, and ease of use of an early moored pCO_2 system developed for buoys in the equatorial Pacific. Like the well-established underway pCO_2 method (Wanninkhof and Thoning, 1993; Feely et al., 1998; Pierrot et al., 2009), this early moored system described by Friederich et al. (1995) and the $MAPCO_2$ system described in Sect. 2.1 combine air–water equilibrators with an infrared (IR) analyzer for CO_2 gas detection. In 2009, the $MAPCO_2$ technology was transferred to Battelle Memorial Institute and is commercially available as the Sealogy® pCO_2 monitoring system. This system is now accessible to the larger scientific community and deployed at over 50 locations in open-ocean, coastal, and coral reef environments, including on NOAA's global moored CO_2 network (www.pmel.noaa.gov/co2/story/Buoys+and+Autonomous+Systems) and Australia's Integrated Marine Observing System (http://imos.org.au).

2.1 Description of $MAPCO_2$ system

The $MAPCO_2$ system includes four separate watertight cases that house the electronics, battery, transmitter, and a reference gas cylinder. The reference gases used on all the PMEL systems are traceable to World Meteorological Organization (WMO) standards and are provided by NOAA's Earth System Research Laboratory (ESRL). In the electronics case are the controls for the system, a memory flash card for data storage, a LI-COR LI-820 CO_2 gas analyzer, and a Sensirion SHT71 relative humidity and temperature sensor. The $MAPCO_2$ also includes an oxygen sensor for internal diagnostic purposes. The LI-820 determines the CO_2 gas concentration by measuring the absorption of IR energy as a sample gas flows through an optical path. The CO_2 concentration is based on the difference ratio in the IR absorption between a reference and a sample optical path. The $MAPCO_2$ uses temperature and relative humidity (RH) to calculate the mole fraction of CO_2 (xCO_2) in air in equilibrium with surface seawater. The LI-820 is calibrated before every measurement using a zero-CO_2 reference and an ESRL standard gas that

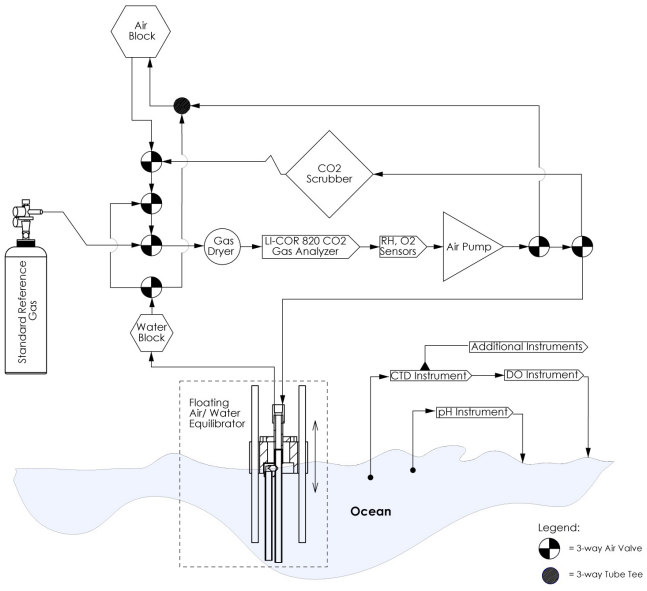

Figure 1. Schematic diagram of main components and sampling paths within the $MAPCO_2$ system. The floating air–water equilibrator is shown in more detail in Fig. 2.

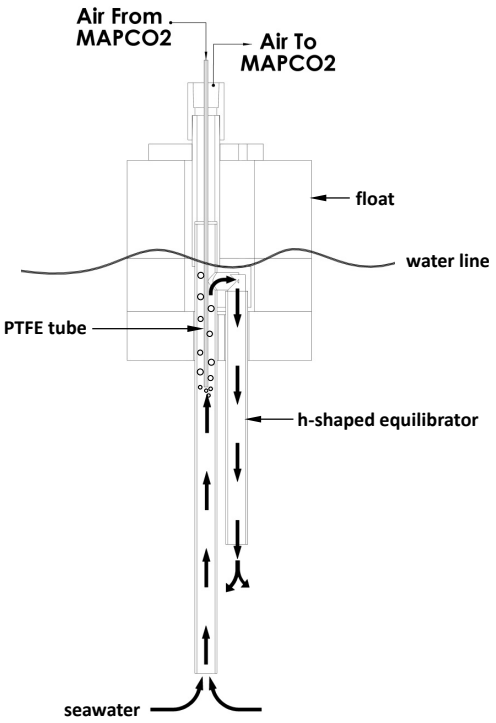

Figure 2. Schematic diagram of the floating air–water equilibrator assembly in the $MAPCO_2$ system during the seawater equilibration cycle. Air is pumped from the $MAPCO_2$ through a PTFE tube and bubbled into the equilibrator. As the bubbles rise through the water, the air comes into equilibrium with the dissolved gases in the surface seawater. The rising air bubbles in the equilibrator also create circulation by pushing water up and over the horizontal leg of the h-shaped equilibrator and out the short leg of the equilibrator. Image is not to scale.

spans the ocean pCO_2 values where the system is deployed. The system also includes a GPS for accurate position and time, an iridium satellite communication link, an airblock deployed approximately 1 m above the ocean surface for atmospheric sampling, and an "h"-shaped bubble equilibrator assembly described by Friederich et al. (1995) (Figs. 1, 2). The equilibrator is the only part of the system in seawater and is made of copper–nickel alloy to prevent bio-fouling.

A schematic diagram of the main components and sampling paths in the $MAPCO_2$ system is shown in Fig. 1. A typical measurement cycle, including in situ calibration and the atmospheric and seawater measurements, takes approximately 20 min. At the beginning of each cycle, the system generates a zero standard by cycling a closed loop of air through a soda lime tube to remove all of the CO_2. This scrubbed air establishes the zero calibration. Next, the system is calibrated with a high standard reference gas, or "span" gas. The value of this gas is set in the $MAPCO_2$ system before deployment (typically $\sim 500\,\mu mol\,mol^{-1}$). The gas flows through the detector for CO_2 analysis and is vented to the atmosphere through the airblock. Once the detector is fully flushed, the flow is stopped and the system returns to atmospheric pressure. Using a two-point calibration from the zero and span values, the LI-820 is optimized for making surface ocean CO_2 measurements.

To make the seawater xCO_2 measurement, the $MAPCO_2$ system equilibrates a closed loop of air with surface seawater in the h-shaped equilibrator, which is mounted in a float designed by PMEL to ensure the optimum depth for equilibration (Fig. 2). The air cycles through the system by pumping air out of flexible polytetrafluoroethylene (PTFE) tubing to approximately 14 cm beneath the surface of the seawater. While the air bubbles through the column of water, the air comes into equilibrium with the dissolved gases in the surface seawater. This air then returns to the system, passing through a silica gel drying agent and the relative humidity sensor. The drying agent is used to prevent condensation in the LI-820 detector and is replaced after each deployment. The air then circulates through the equilibrator again. The closed loop of air repeats this cycle for 10 min. The rising air bubbles in the equilibrator create seawater circulation in the equilibrator by pushing the water up and over the horizontal leg of the equilibrator and out the short leg of the equilibrator (Fig. 2). This draws new water into the long leg of the equilibrator, ensuring that the recirculated air is always in contact with new seawater. After 10 min of equilibration, the pump is stopped and the LI-820 values are read on the air sample at 2 Hz for 30 s and averaged to give the seawater xCO_2 measurement. This is a measurement of integrated seawater CO_2 levels during the 10 min equilibration time.

After the equilibrator reading, a MBL air reading is made by drawing air in through the airblock, partially drying it, and

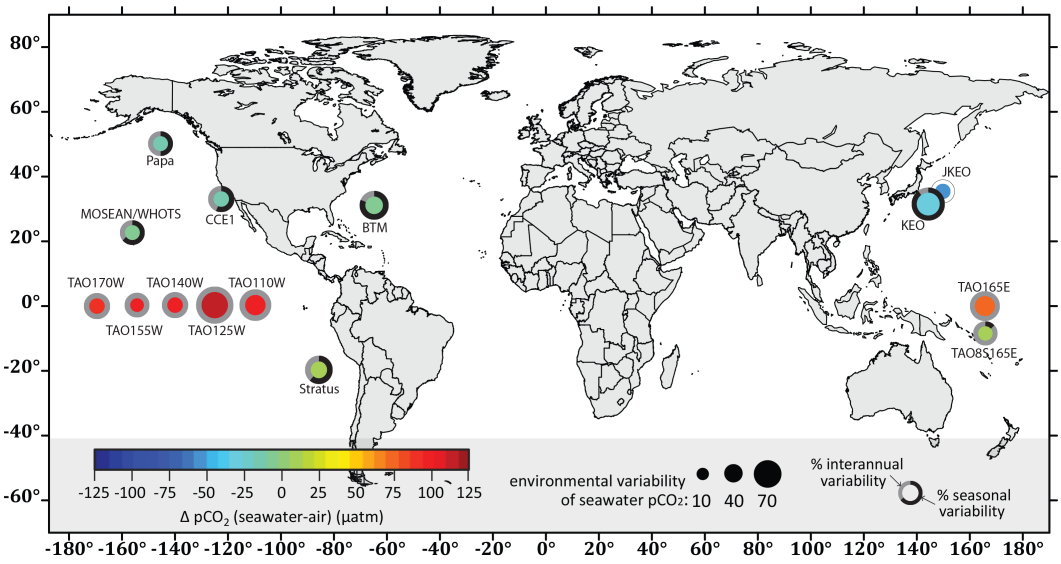

Figure 3. Location of open-ocean moorings in the MAPCO$_2$ data set. Inner circle color illustrates the mean ΔpCO_2 of the finalized data at that location. Inner circle size is relative to the environmental variability in the time series defined here as the standard deviation of seawater pCO_2 values. The outer ring shows the proportion of environmental variability in seawater pCO_2 due to the seasonal cycle (black) and interannual variability (gray). Seasonal variability is defined as the mean seasonal peak amplitude, and interannual variability is the mean Δ of annual mean values. Seasonal and interannual variability cannot be quantified at JKEO with a time series of < 1 year and is represented here by an outer ring with no color.

passing it through the LI-820. Once the LI-820 path has been flushed, the flow is stopped and a 30 s average reading is collected. All measurements and calibrations are made at atmospheric pressure. The seawater CO_2 measurement occurs approximately 17 min after the start of the measurement cycle followed by the air CO_2 measurement 2 min later. Response time of the MAPCO$_2$ is dictated by the length of the full 20 min measurement cycle, and in fast mode the MAPCO$_2$ system can measure atmospheric and seawater CO_2 once every 30 min.

Different types of sensors are used throughout the system for analytical, troubleshooting, and data quality control purposes. Additional parameters measured in each cycle (i.e., zero, span, equilibrator, and air) include temperature, pressure, relative humidity, and oxygen. Other sensors can also be integrated into the MAPCO$_2$, including CTD (conductivity, temperature, and depth) instruments with auxiliary sensors attached (e.g., dissolved oxygen, fluorescence, turbidity) and pH sensors. The raw data collected by the MAPCO$_2$ and integrated sensors are stored on a memory flash card, and averaged data from each 3-hourly cycle are telemetered from the buoy via the iridium satellite communications system. This communications system also enables the user to control the MAPCO$_2$ remotely. The user can determine the sampling frequency and other variables, but the MAPCO$_2$ is nominally designed to make CO_2 measurements every 3 h with daily data transmissions for at least 400 days.

PMEL's MAPCO$_2$ systems have been deployed on open-ocean buoys starting in 2004 with the establishment of NOAA's global moored CO_2 network and the efforts of numerous partners (see Acknowledgements). Table 1 lists the mooring coordinates and dates of CO_2 time series operation; Fig. 3 illustrates the locations, number of measurements, and average ΔpCO_2 (sea–air) from the 14 surface CO_2 buoys included in this data set. These mooring ΔpCO_2 observations are consistent with results of a synthesis of underway observations reported by Takahashi et al. (2009). Other than the Bermuda Testbed Mooring (BTM) and Japanese Kuroshio Extension Observatory (JKEO) time series, which have been discontinued, and the Multi-disciplinary Ocean Sensors for Environmental Analyses and Networks (MOSEAN) buoy, which was moved approximately 20 km to the new Woods Hole Oceanographic Institution (WHOI) Hawaii Ocean Time-Series Station (WHOTS) location, the MAPCO$_2$ time series shown in Fig. 3 and Table 1 continue to be maintained. Seven of the 14 CO_2 buoys are located in the equatorial Pacific on the Tropical Atmosphere Ocean (TAO) array. Additional open-ocean MAPCO$_2$ sites maintained by PMEL now exist in the North Atlantic, northern Indian, and Southern oceans (see http://www.pmel.noaa.gov/co2/story/Buoys+and+Autonomous+Systems); however, they have been deployed since 2011 and are not included in the finalized data set presented here.

2.2 Data reduction and processing

The IR analyzer has a nonlinear response to CO_2, but that response is very well characterized by the manufacturer.

Table 1. Details of each CO_2 mooring time series including name, coordinates (decimal degrees), and dates of operational CO_2 measurements.

Abbreviation	Full Name	Latitude	Longitude	Year established	Current Status
MOSEAN	Multi-disciplinary Ocean Sensors for Environmental Analyses and Networks	22.8	−158.1	2004	moved to WHOTS in 2007
WHOTS	WHOI Hawaii Ocean Time-Series Station	22.7	−158.0	2007	ongoing
BTM	Bermuda Testbed Mooring	31.5	−64.0	2005	discontinued in 2007
Papa	Papa	50.1	−144.8	2007	ongoing
KEO	Kuroshio Extension Observatory	32.3	144.6	2007	ongoing
JKEO	Japanese Kuroshio Extension Observatory	37.9	146.6	2007	discontinued in 2007
CCE1	California Current Ecosystem 1	33.5	−122.5	2008	ongoing
Stratus	Stratus	−19.7	−85.6	2006	ongoing
TAO110W	Tropical Atmosphere Ocean 0°, 110° W	0.0	−110.0	2009	ongoing
TAO125W	Tropical Atmosphere Ocean 0°, 125° W	0.0	−125.0	2004	ongoing
TAO140W	Tropical Atmosphere Ocean 0°, 140° W	0.0	−140.0	2004	ongoing
TAO155W	Tropical Atmosphere Ocean 0°, 155° W	0.0	−155.0	2010	ongoing
TAO170W	Tropical Atmosphere Ocean 0°, 170° W	0.0	−170.0	2005	ongoing
TAO165E	Tropical Atmosphere Ocean 0°, 165° E	0.0	165.0	2010	ongoing
TAO8S165E	Tropical Atmosphere Ocean 8° S, 165° E	−8.0	165.0	2009	ongoing

LI-COR has a function built into their firmware that accounts for the nonlinear response and linearizes the output data. The linear function is calibrated prior to each atmospheric and seawater measurement with the zero- (intercept) and high-CO_2 standard reference gas (slope). The accuracy of the linearized, calibrated output is confirmed prior to deployment by analyzing a range of intermediate-CO_2 standards in our laboratory.

The primary check of accuracy before and after deployment is a comparison to ESRL CO_2 standards traceable to WMO standards, typically six standards that range from 0 to $< 800\ \mu mol\ mol^{-1}$. Systems are not certified for deployment until values are within the expected range of the standards that span the typical seawater CO_2 values at the mooring location (typically within $2\ \mu mol\ mol^{-1}$). A comparison to the underway pCO_2 system in the lab is then done to assess stability of the measurements over at least 1 week. During this test, each $MAPCO_2$ is tested in a seawater tank in the lab against another $MAPCO_2$ system and a General Oceanics 8050 underway pCO_2 system that are permanently mounted for continuous sampling in the seawater tank. The standard $MAPCO_2$ is regularly compared to the underway system, which is calibrated every 8 h using four standard reference gases from approximately 0 to $1000\ \mu mol\ mol^{-1}$. Laboratory testing of the $MAPCO_2$ systems suggests instrument precision is $< 0.6\ \mu mol\ mol^{-1}$ for xCO_2 values between 100 and $600\ \mu mol\ mol^{-1}$.

When the $MAPCO_2$ is recovered from the field, the system is compared against six gas standards to verify accuracy, and the high-frequency raw data stored on the internal memory flash card are downloaded to a local database. The high-frequency raw data from each 3-hourly cycle are then used for final processing of each data set. Averaged xCO_2 (wet) seawater and atmospheric measurements (defined in Table 2) from each cycle are calculated starting with the raw detector counts using the published LI-COR function. The span gas coefficients used in the function during post-processing are derived from the linear regression between the calibration coefficients and the corresponding LI-820 temperature measurements acquired during the span cycle over the course of the deployment. This post-deployment reprocessing facilitates the accurate calculation of xCO_2 (wet) values from the raw detector counts when rare miscalibrations occur, resulting in erroneous coefficients during the deployment. Since the LI-820 is calibrated prior to each cycle of xCO_2 (wet) measurements using the zero- and high-CO_2 standard reference gas, detector drift is negligible. This is confirmed by a mean difference between corrected and original raw data of $-0.02\ \mu mol\ mol^{-1}$.

Data are quality-controlled and flagged according to the SOCAT guidelines (Pfeil et al., 2013). For pCO_2 mooring purposes, we use three quality flags (QFs): a flag value of 2 represents an acceptable measurement, 3 is a questionable measurement, and 4 is a bad measurement. A measurement can be questionable for a variety of reasons often revealed by $MAPCO_2$ system diagnostic information (e.g., low equilibrator pressure causing incomplete seawater equilibration), and the reasoning for each flag is included in the metadata QC log so the end user can decide whether or not to use questionable data. Prior to a data QC software update in June 2013, xCO_2 values flagged as bad (QF = 4) were still included in the published data sets, but after the software update bad values are replaced with −999. Other parameters published in the data sets that do not have an associated flag, such as sea surface temperature (SST) and sea surface salinity (SSS), are given a value of −999 or −9.999 when the measurement is missing or bad.

Table 2. Final data variable names and descriptions.

Variable name	Description	Units	Equation (if applicable)
Mooring	mooring name as shown in Fig. 2 and Table 1	character string	
Latitude	average latitude during deployment	decimal degrees	
Longitude	average longitude during deployment	decimal degrees	
Date	date of measurement in UTC	MM/DD/YYYY	
Time	time of measurement in UTC	HH:MM	
xCO2_SW_wet	mole fraction of carbon dioxide in air in equilibrium with surface seawater at SST and humidity	$\mu mol\ mol^{-1}$	
xCO2_SW_QF	primary flag associated with seawater xCO_2 measurement	WOCE standards[a]	
H2O_SW	mole fraction of water in gas from equilibrator	$\mu mol\ mol^{-1}$	
xCO2_Air_wet	mole fraction of carbon dioxide in air at ~ 1.5 m above the sea surface at sample humidity	$\mu mol\ mol^{-1}$	
xCO2_SW_QF	primary flag associated with air xCO_2 measurement	WOCE standards[a]	
H2O_Air	mole fraction of water in air	$\mu mol\ mol^{-1}$	
Licor_Atm_Pressure	atmospheric pressure at ~ 1.5 m above the sea surface	hPa	
Licor_Temp	licor temperature	°C	
Percent_O2[b]	% oxygen in surface seawater divided by % oxygen in air at ~ 1.5 m above the sea surface	%	
SST[c]	sea surface temperature	°C	
SSS[c]	sea surface salinity		
xCO2_SW_dry	mole fraction of carbon dioxide in dry air in equilibrium with surface seawater	$\mu mol\ mol^{-1}$	1
xCO2_Air_dry	mole fraction of carbon dioxide in dry air at ~ 1.5 m above the sea surface	$\mu mol\ mol^{-1}$	1
fCO2_SW_sat	fugacity of carbon dioxide in wet air (100 % humidity) in equilibrium with surface seawater	µatm	4
fCO2_Air_sat	fugacity of carbon dioxide in wet air (100 % humidity) at ~ 1.5 m above the sea surface	µatm	4
dfCO2	fCO2_SW_sat – fCO2_Air_sat	µatm	
pCO2_SW_sat[d]	partial pressure of carbon dioxide in wet air (100 % humidity) in equilibrium with surface seawater	µatm	5
pCO2_Air_sat[d]	partial pressure of carbon dioxide in wet air (100 % humidity) at ~ 1.5 m above the sea surface	µatm	5
dpCO2[d]	pCO2_SW_sat – pCO2_Air_sat	µatm	

Notes: [a] SOCAT flags used in this data set: 2 = acceptable measurement; 3 = questionable measurement; 4 = bad measurement (note: bad data values are reported in the final data file submitted to CDIAC prior to QC software upgrade in June 2013 but reported as −999 in files submitted after the upgrade). [b] Oxygen measured in the $MAPCO_2$ system is exposed to air and likely modified within the system prior to measurement. Rapid changes in oxygen are not properly captured using this method. This data should not be used as a quantitative measure of oxygen. [c] Usually measured by other academic partners at each site. See metadata for each deployment for details on SST and SSS measurements. [d] $pCO2$ only presented in data sets submitted to CDIAC after June 2013 when QC software was upgraded to include this calculation. Data users of earlier data sets can calculate $pCO2$ as defined in Eq. (4).

As a final check of the data QC process, atmospheric xCO_2 (dry) data are compared to MBL data from the GLOBALVIEW-CO2 product and the $MAPCO_2$ systems deployed before and after the deployment of interest (GLOBALVIEW-CO2, 2013). When a $MAPCO_2$ system is recovered and a new system deployed, there is typically some overlap in measurements at each location. In cases when there is an offset in air xCO_2 values between systems at the same location, which is often corroborated by an offset from the GLOBALVIEW-CO2 MBL time series as well, a correction (typically $\leq 3\ \mu mol\ mol^{-1}$) is applied to the atmospheric and seawater xCO_2 (wet) values. This correction is noted in the metadata and can be removed by the data user if desired. The GLOBALVIEW-CO2 MBL data set serves as a useful and unifying comparison data set, especially since other in situ comparison data are often lacking. As we build $MAPCO_2$ time series at each of these locations, we start to build an understanding of how the $MAPCO_2$ observations typically compare to the MBL data set. For example, winter atmospheric xCO_2 values measured by our $MAPCO_2$ systems at Papa are consistently lower than MBL values (Fig. 4a).

Post-QC calculation of pCO_2 and fCO_2 (fugacity of CO_2) are made according to recommendations of the underway pCO_2 community (Pierrot et al., 2009). However, $MAPCO_2$ measurements of xCO_2 vary from the underway pCO_2 method. The $MAPCO_2$ system uses the LI-820 and the RH to report the mole fraction of CO_2 in air in equilibrium with surface seawater, called xCO_2 (wet). This "partially wet" measurement typically has a RH of ~ 75 % (seawater and atmospheric samples), which is not completely dried as in the underway pCO_2 method, due to lack of drying methods available for extended autonomous operation. However, since we measure RH and temperature of the sample air stream exiting the LI-820, we can calculate xCO_2 (dry) using Eqs. (1)–(3). First, xCO_2 in dry air is calculated by

$$xCO_2\,(\text{dry}) = xCO_2\,(\text{wet}) \times \frac{P_{\text{Licor}}}{P_{\text{Licor}} - VP_{\text{Licor}}}, \quad (1)$$

where xCO_2 (wet) is the LI-820 measured concentration ($\mu mol\ mol^{-1}$), P_{Licor} is the pressure of the atmospheric and seawater samples measured in the LI-820 (kPa) and considered atmospheric pressure, and VP_{Licor} is the vapor pressure in the LI-820 (kPa). RH measurements of the air samples exiting the LI-820 are used to calculate VP_{Licor} in Eq. (1) using the following as defined by Buck (1981) and LI-COR for the IR analyzers:

$$VP_{\text{sat}} = (0.61121)(1.004)e^{\left(\frac{17.502 \times T_{\text{RH}}}{240.97 + T_{\text{RH}}}\right)} \quad (2)$$

$$VP_{\text{Licor}} = (\text{RH}_{\text{sample}} - \text{RH}_{\text{span}}) \times \frac{VP_{\text{sat}}}{100}, \quad (3)$$

where VP_{sat} is the saturation vapor pressure of the RH sensor cell (kPa); T_{RH} is the temperature of the RH sensor (°C);

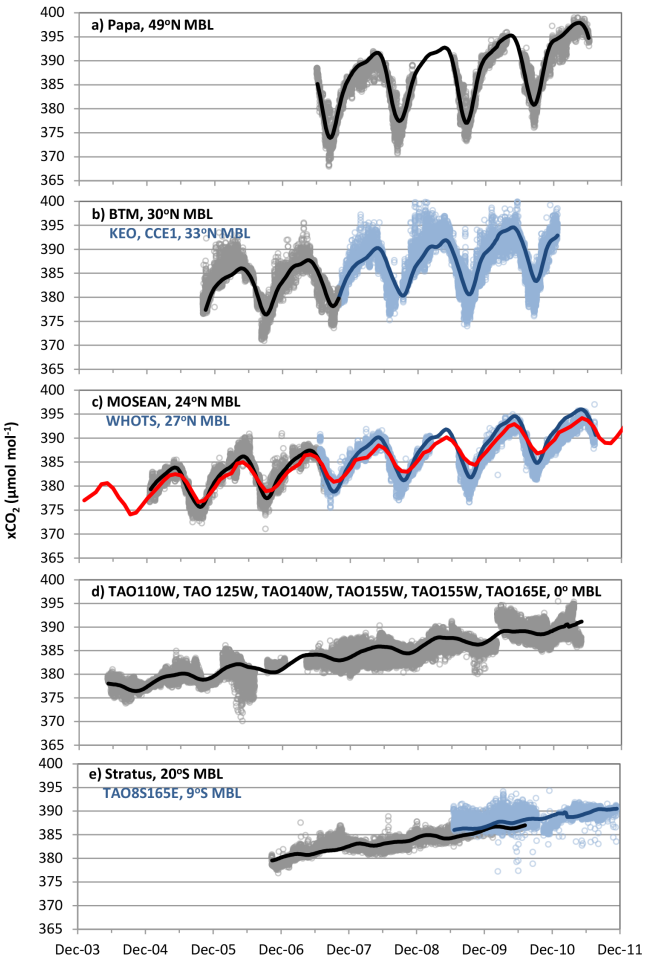

Figure 4. $MAPCO_2$ and GLOBALVIEW-CO2 MBL atmospheric xCO_2 (µmol mol^{-1}) presented by latitude: **(a)** Papa $MAPCO_2$ (gray points) and MBL at 49° N (black line); **(b)** BTM $MAPCO_2$ (gray points) and MBL at 30° N (black line), KEO and CCE1 $MAPCO_2$ (blue points) and MBL at 33° N (blue line); **(c)** MOSEAN $MAPCO_2$ (gray points) and MBL at 24° N (black line), WHOTS $MAPCO_2$ (blue points) and MBL at 27° N (blue line), and Mauna Loa Observatory atmospheric xCO_2 (red line); **(d)** six equatorial $MAPCO_2$ buoys (gray points) and MBL at 0° (black line); and **(e)** Stratus $MAPCO_2$ (gray points) and MBL at 20° S (black line), TAO8S165E $MAPCO_2$ (blue points) and MBL at 9° S (blue line). MBL data from GLOBALVIEW-CO2 (2013). Mauna Loa Observatory monthly mean data from Pieter Tans, NOAA/ESRL (http://www.esrl.noaa.gov/gmd/ccgg/trends/), and Ralph Keeling, Scripps Institution of Oceanography (http://scrippsco2.ucsd.edu/).

RH_{sample} is the RH of the air sample (%); and RH_{span} is the RH of the span (%), i.e., the background RH level for the system. Equation (2) is a calculation of vapor pressure optimized for the temperature interval of −20 to 50 °C as defined by Buck (1981). This equation includes coefficients for calculating VP_{sat} with an enhancement factor (a correction for dealing with moist air as a function of temperature and pressure) of 1.004 for 20 °C and 1000 mb (Buck, 1981). VP_{sat} and RH of the air sample are then used to calculate VP_{Licor}. Once the VP_{Licor} is known, the dilution effect can then be removed from the partially wet xCO_2 measurement using Eq. (1) to calculate xCO_2 (dry).

Since the $MAPCO_2$ equilibration occurs directly in the ocean, it does not require the warming correction necessary for underway pCO_2 systems. Therefore, pCO_2 in wet air (100 % saturation) in equilibrium with the surface seawater is calculated by

$$pCO_2(\text{sat}) = xCO_2(\text{dry}) \times (P_{\text{Licor}} - pH_2O), \quad (4)$$

where P_{Licor} is atmospheric pressure for the atmospheric and surface seawater samples (atm) and pH_2O is the water vapor pressure (atm) at equilibrator temperature as defined by Weiss and Price (1980). fCO_2 in wet air (100 % saturation) in equilibrium with the surface seawater is calculated by

$$fCO_2(\text{sat}) = pCO_2(\text{sat}) \times e^{\left[\frac{P_{\text{Licor}} \times (B_{11} + 2\delta_{12})}{R \times T}\right]}, \quad (5)$$

where the ideal gas constant $R = 82.0578\,\text{cm}^3\,\text{atm}\,\text{mol}^{-1}\,\text{K}^{-1}$, T is SST (K) from the CTD, and the B_{11} virial coefficient and δ_{12} cross-virial coefficient for CO_2 are as defined by Weiss (1974). The raw CO_2 data, temperature, salinity, and pressures are included in all published $MAPCO_2$ data sets so other data users can recalculate xCO_2, fCO_2, and pCO_2. Additional parameters included with the pCO_2 mooring data set are listed and described in Table 2.

2.3 Uncertainty of pCO_2 measurements

Precision and accuracy of the $MAPCO_2$ measurements have been assessed in both laboratory and field settings. As stated in Sect. 2.2, the precision of the $MAPCO_2$ system in a laboratory setting is 0.6 µmol mol^{-1}. Standard deviation of the high-frequency raw data (∼ 58 repeated measurements over 30 s) in the field is a good assessment of the in situ precision of the $MAPCO_2$ system. Mean standard deviation of the raw data from the 14 buoy time series presented here is 0.7 µmol mol^{-1} for seawater xCO_2 and 0.6 µmol mol^{-1} for air xCO_2, which is similar to precision measured in the laboratory. While estimating accuracy in a laboratory setting is feasible, the more-desired estimate of in situ accuracy is difficult to obtain due to the limited availability of validation samples for comparison and the mismatch in space and time of these validation samples compared to the $MAPCO_2$ measurements. These issues related to accuracy will be discussed in more detail below. In this section, we present $MAPCO_2$-estimated in situ precision, accuracy, and uncertainty, which we define as the overall error of the measurement encompassing instrument precision and accuracy as well as propagation of error.

Propagation of error must be considered when calculations are based on variables with individual uncertainties. These

Table 3. Sources of error for the calculation of xCO_2 (dry) at atmospheric pressure = 101 kPa, RH_{sample} = 75 %, RH_{span} = 30 %, SST = 25 °C, SSS = 35, and xCO_2 (wet) = 375 µmol mol^{-1}. Total estimated precision and accuracy are calculated using the root-sum-of-squares method (RSS): $RSS = \left(\sum a^2\right)^{1/2}$.

Sources of error	Variable precision (±)	Effect on precision of final calculation (a)	Variable accuracy (±)	Effect on accuracy of final calculation (a)
VP_{Licor} calculation				
VP_{sat} (kPa)	0.019[a]	0.009	0.057[a]	0.026
RH_{sample}	0.1[b]	negligible	3.0[b]	0.1
RH_{span}	0.1[b]	negligible	3.0[b]	0.1
Assumption that $VP_{RH} = VP_{Licor}$				0.052
Total estimated error: VP_{Licor}		0.009		0.153
xCO_2 (dry) calculation				
xCO_2 (wet) (µmol mol^{-1})	0.7[c]	0.7	1.5[c]	1.5
P_{Licor} (kPa)	0.001[b]	negligible	0.010[b]	negligible
VP_{Licor} (kPa) (calculated above)	0.009	0.034	0.153	0.585
Total estimated error: xCO_2 (dry)		0.7		1.6

Notes: [a] Error calculated using manufacturer-estimated error for T_{RH} of ±0.1 °C precision and ±0.3 °C accuracy (see Eq. 2). [b] Error reported by manufacturer. [c] Precision estimate based on standard deviation of the high-frequency raw data (~ 58 repeated measurements over 30 s) in the field; accuracy estimate based on pre-deployment testing in the laboratory. Negligible indicates value < significant digits of variable.

types of errors that impact the calculated pCO_2 and fCO_2 values have been assessed for underway pCO_2 systems and are typically small (< 0.1 µatm) with minimal impact to the overall uncertainty when combined with the larger uncertainty (< 2 µatm) in the actual xCO_2 measurement (Feely et al., 1998; Wanninkhof and Thoning, 1993; Pierrot et al., 2009). However, we utilize a different method to calculate xCO_2 (dry) for the $MAPCO_2$ system, as discussed in Sect. 2.1, so it is important to address the potential error in this new method. The RH measurements used to calculate xCO_2 (dry) have separate precisions and accuracies that can propagate through Eqs. (1)–(3) (Table 3). The total estimated precision and accuracy of xCO_2 (dry) are calculated by summing each variable's precision and accuracy using the root-sum-of-squares method. As presented in Table 3, propagation of all the errors from the separate variables does not cause the precision of calculated xCO_2 (dry) to differ from measured xCO_2 (wet) and results in a small impact to the accuracy (0.1 µmol mol^{-1}).

In addition to the propagation of error, an estimate of in situ accuracy is key to determining the overall uncertainty of the $MAPCO_2$ system. The GLOBALVIEW-CO2 data product maintained by NOAA ESRL can be used as one data set for comparison to the $MAPCO_2$ air xCO_2 (dry) measurements (GLOBALVIEW-CO2, 2013). Figure 4 shows 3-hourly atmospheric $MAPCO_2$ measurements and biweekly atmospheric CO_2 values from the MBL layer of GLOBALVIEW-CO2 at the latitude closest to each $MAPCO_2$ location. Atmospheric $MAPCO_2$ data presented here are in the finalized, processed form as described in Sect. 2.2. Both MBL and $MAPCO_2$ data capture seasonal variability and long-term trends, but, as expected, high-frequency $MAPCO_2$ measurements show short-term variability typically deviating from the smoothed MBL data product by < 5 µmol mol^{-1} (Fig. 4). The Mauna Loa atmospheric CO_2 record is also shown in Fig. 4c and provides a reference for illustrating the larger seasonal variability in the lower atmosphere directly influenced by the presence of the ocean's surface. For the time series longer than 2 years, growth rates of the 3-hourly $MAPCO_2$ and biweekly MBL atmospheric CO_2 are presented in Table 4. Atmospheric CO_2 growth rates observed by five of the seven mooring time series differ from the MBL data by ≤ 0.1 µmol mol^{-1} yr^{-1}, suggesting that the finalized $MAPCO_2$ observations are consistent with other atmospheric data products generated using different methods.

$MAPCO_2$ and MBL data are compared in more detail in Table 5. This includes descriptive statistics of the finalized, processed atmospheric data in addition to pre-finalized data prior to any adjustments or offsets. The 3-hourly $MAPCO_2$ measurement that is closest in time to the biweekly MBL estimate is used to calculate the Δ ($MAPCO_2$–MBL). Pre-QC $MAPCO_2$ data show a slight negative bias (−1.5 ± 2.4 µmol mol^{-1}) to MBL values (Table 5). The mean difference between finalized $MAPCO_2$ data and MBL values is smaller (−0.3 ± 1.7 µmol mol^{-1}) due to the application of occasional offsets during data QC described in Sect. 2.2. Standard deviations likely reflect the natural variability in atmospheric CO_2 at the sea surface illustrated in Fig. 4. Low standard error of the mean and low confidence

Table 4. Growth rate of GLOBALVIEW-CO2 MBL and $MAPCO_2$ atmospheric xCO_2 time series over the time period of the data sets listed in Table 5 (GLOBALVIEW-CO2, 2013). For mooring time series locations see Fig. 3.

	Growth rate ($\mu mol\ mol^{-1}\ yr^{-1}$)	
Time series > 2 years	MBL	$MAPCO_2$
Papa	3.1	3.1
KEO	1.7	1.1
MOSEAN/WHOTS	2.0	1.6
TAO125W	1.9	2.0
TAO140W	1.9	1.9
TAO170W	1.9	1.9
Stratus	1.8	1.9

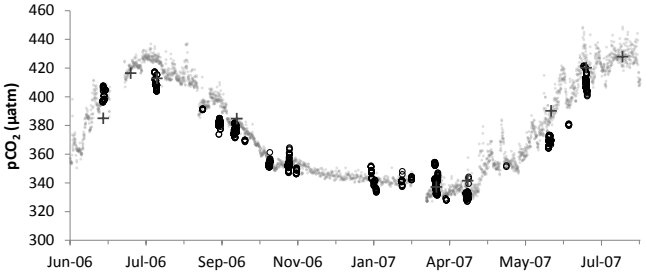

Figure 5. Seawater pCO_2 values from BTM $MAPCO_2$ (gray points), Bermuda Atlantic Time-series Study (BATS) discrete (plus signs), and R/V *Atlantic Explorer* underway (open circles) used in the Table 5 statistics. BATS data from Bermuda Institute of Ocean Sciences, bats.bios.edu. *Atlantic Explorer* data from Bermuda Institute of Ocean Sciences, http://cdiac.ornl.gov/oceans/CARINA/.

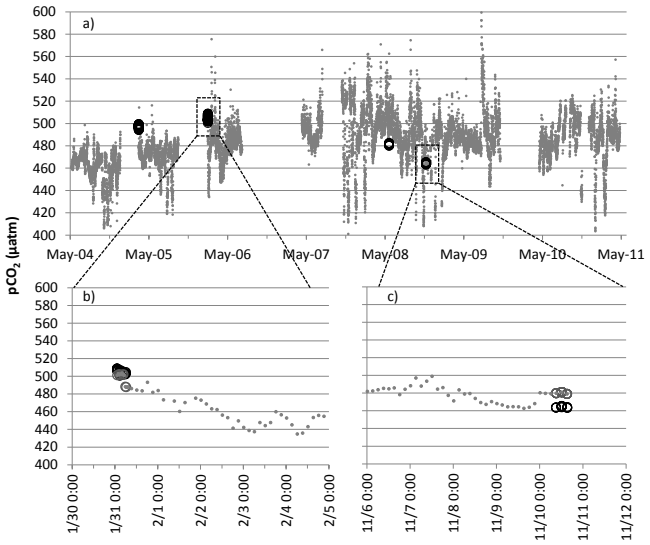

Figure 6. **(a)** TAO125W surface seawater $MAPCO_2$ observations (gray points) for the entire time series at this location with average R/V *Ka'imimoana* underway pCO_2 data within 10 km and 10 min of the $MAPCO_2$ measurements (black open circles). Two examples of comparison data over 1-week time series are shown in panels **(b)** and **(c)**, with $MAPCO_2$ measurements corresponding to the average underway observations illustrated in gray open circles. Selection boxes in **(a)** are not to scale of actual axes in **(b)** and **(c)** panels. *Ka'imimoana* data from NOAA PMEL, http://cdiac.ornl.gov/oceans/VOS_Program/kaimimoana.html.

level values reported for the atmospheric comparison in Table 5 suggest strong statistical significance in the mean $MAPCO_2$–MBL values.

While environmental variability may introduce some error to the $MAPCO_2$ and MBL air comparison, the resulting mean differences in the atmospheric data are likely due primarily to uncertainty in the measurements, which in this case we associate with the $MAPCO_2$ system. However, surface ocean pCO_2 exhibits large temporal and spatial variability. For example, it is common to observe variability in underway pCO_2 measurements from the R/V *Atlantic Explorer* of approximately 10 µatm within 10 km of BTM over a period of 3 h (Fig. 5). We observe even larger variability in the eastern equatorial Pacific, with changes up to 50 µatm over a period of 3 h and > 100 µatm over the course of a day (Fig. 6a). This patchiness can create errors in comparing $MAPCO_2$ measurements to ship-based measurements made at safe distance from the surface buoy. In Fig. 6b, for example, the difference between the TAO125W $MAPCO_2$ and underway measurements from the R/V *Ka'imimoana* (made within 10 km and 10 min of the $MAPCO_2$ measurement) start at ±2 µatm on 31 January 2006 at 14:00:00, but as the ship begins to leave the surface buoy 6 h later the measurements diverge as the $MAPCO_2$ starts to detect a decreasing trend in surface seawater pCO_2 values at the buoy location that persists for the next 8 days. In another example shown in Fig. 6c, the 15 µatm difference between the $MAPCO_2$ and underway system observed on 10 November 2008 is similar to the daily variability observed at the buoy in the 4 days prior to arrival of the *Ka'imimoana* and could reflect true differences observed by the underway and $MAPCO_2$ systems located 1–7 km apart. These examples highlight the difficulty of separating environmental variability and instrument uncertainty in these types of comparison exercises.

In order to minimize environmental variability while maximizing sample size for descriptive statistics, we use discrete measurements made within 10 km and 1.5 h and averaged underway pCO_2 measurements made within 10 km and 10 min of the $MAPCO_2$ system measurements for the seawater pCO_2 comparison analysis. While underway and $MAPCO_2$ systems utilize similar methodology, discrete pCO_2 presented in Table 5 is calculated from measurements of dissolved inorganic carbon (DIC) and total alkalinity (TA) using the program CO2SYS developed by Lewis and Wallace (1998) with the constants of Lueker et al. (2000). Typical error in calculated pCO_2 using this method is < 5 %. Only finalized seawater $MAPCO_2$ data are used for the descriptive

Table 5. Descriptive statistics of Δ ($MAPCO_2$ measurement – comparison measurement). The $MAPCO_2$ measurements (both pre- and post-offset if applied during data QC) are compared to biweekly GLOBALVIEW-CO2 MBL values from the latitude nearest to average buoy location, single discrete measurements made within 10 km and 1.5 h, and averaged underway pCO_2 measurements made within 10 km and 10 min of the $MAPCO_2$ system measurement. Standard error is the standard error of the mean, and confidence intervals illustrate that with a 95 % probability the actual population mean = sample mean ± confidence interval.

	n	Mean	Standard error	Standard deviation	Confidence interval (95 %)
$MAPCO_2$ air xCO_2 (dry) comparison to MBL[a] air (μmol mol^{-1})					
Data prior to QC (estimate of $MAPCO_2$ system in situ accuracy)	1823	−1.5	0.1	2.4	0.1
Finalized data (estimate of finalized $MAPCO_2$ data accuracy)	1823	−0.3	< 0.1	1.7	0.1
$MAPCO_2$ seawater pCO_2 comparison to calculated pCO_2 (μatm) from discrete DIC, TA					
WHOTS vs. HOTS[b]	7	0.1	1.4	3.7	3.4
BTM vs. BATS[c]	9	1.3	1.9	5.6	4.3
Papa vs. Station P[d]	10	−0.4	2.0	6.2	4.5
$MAPCO_2$ seawater pCO_2 comparison to underway pCO_2 (μatm)					
BTM vs. *Atlantic Explorer*[e]	76	1.8	0.5	4.8	1.1
TAO125W vs. *Ka'imimoana*[f]	16	−3.3	3.8	15.2	8.1
TAO140W vs. *Ka'imimoana*[f]	13	2.1	2.3	8.3	5.0

Notes on data sources and archives: [a] GLOBALVIEW-CO2 marine boundary layer (MBL) data source: NOAA Earth System Research Laboratory, http://www.esrl.noaa.gov/gmd/ccgg/globalview/co2/co2_intro.html (GLOBALVIEW-CO2, 2013). [b] Hawaii Ocean Time-Series (HOTS) data source: University of Hawaii, hahana.soest.hawaii.edu/hot. [c] Bermuda Atlantic Time-series Study (BATS) data source: Bermuda Institute of Ocean Sciences, http://bats.bios.edu. [d] Station P data source: University of Washington and NOAA PMEL. [e] *Atlantic Explorer* data source: Bermuda Institute of Ocean Sciences, http://cdiac.ornl.gov/oceans/CARINA/. [f] *Ka'imimoana* data source: NOAA PMEL, http://cdiac.ornl.gov/oceans/VOS_Program/kaimimoana.html.

statistics presented in Table 5. Unlike the descriptive statistics for the $MAPCO_2$ air comparisons, the statistics that result from using $MAPCO_2$ seawater measurements pre-MBL offset are not statistically different than the finalized, post-MBL offset statistics presented in Table 5. This could be due to the large natural variability in seawater pCO_2 compared to atmospheric CO_2.

Agreement between discrete and mooring surface ocean pCO_2 measurements is within 1.3 μatm (mean Δ in Table 5; BTM example in Fig. 5). Although more discrete measurements have been made at these and other mooring locations, this comparison is based on discrete samples restricted to within 10 km and 1.5 h of the $MAPCO_2$ system measurements with $n > 5$. Even with these restrictions, it is likely that environmental variability is not completely removed and is reflected in the mean Δ standard deviations of 3.7–6.2 μatm (Table 5). The small sample sizes (≤ 10 at each site) also resulting from these restrictions create large uncertainty in mean Δ values, with standard error and confidence levels exceeding mean Δ values. This analysis shows promising results with a close agreement between discrete and $MAPCO_2$ measurements; however, more discrete samples will need to be collected within 10 km and 1.5 h of $MAPCO_2$ system measurements in order to improve the statistical significance of the seawater pCO_2 comparison.

Sample sizes are larger ($13 \leq n \leq 76$) for the comparison between underway and $MAPCO_2$ measurements at the BTM, TAO125W, and TAO140W locations. While underway measurements exist at other equatorial Pacific mooring locations, comparisons within 10 km and 10 min are restricted to TAO125W and TAO140W due to the large gaps in pCO_2 mooring data, the infrequent mooring-servicing ship visits to each site (∼ once every 1–1.5 years), and the necessity for the mooring-servicing ship to leave for the next station before the $MAPCO_2$ system has gone through a few cycles and measurements have stabilized. Even with these challenges, there are 76 comparison samples at BTM during the two buoy deployments in 2006–2007 (Fig. 5). These measurements show a mean Δ of 1.8 ± 4.8 μatm with a low confidence interval of 1.1, indicating strong statistical significance ($p < 0.05$) that the actual mean Δ is between 0.7 and 2.9 μatm (Table 5). Standard deviations of the difference between the BTM versus discrete (5.6) and underway (4.8) measurements are similar, which may be reflective of the environmental variability in this region of the surface ocean. Mean Δ in the equatorial Pacific is higher (-3.3 ± 15.2 μatm at TAO125W and 2.1 ± 8.3 μatm at TAO140W), but statistical significance of these values is low due to the lower sample sizes and higher environmental variability in this region (Fig. 3). The largest standard deviation in mean Δ of 15.2 is at TAO125W, which is the site that exhibits the largest natural variability (i.e., total

range of ∼200 µatm, Fig. 6a) in surface seawater pCO_2 of the open-ocean mooring data sets compared in Table 5.

The $MAPCO_2$ system has also been involved in two independent ocean pCO_2 instrument intercomparisons. During an Alliance for Coastal Technologies demonstration project, the difference between the $MAPCO_2$ system and an underway pCO_2 system was -9 ± 8 µatm in coastal Washington, USA waters and -3 ± 9 µatm in coral reef waters of Kaneohe Bay, Hawaii, USA (Schar et al., 2010). Separating environmental variability from instrument uncertainty in this case is challenging. Small-scale environmental variability (i.e., meters) due to natural spatial patchiness of pCO_2 was determined to be 10–15 µatm at the coastal site and < 2 µatm at the coral site and may account for much of the difference observed between the $MAPCO_2$ and reference measurements. An intercomparison between buoy and underway pCO_2 systems held at the National Research Institute of Fishery Engineering in Hasaki, Kamisu city, Ibaraki, Japan, was done in the more controlled environment of an indoor seawater pool (UNESCO, 2010). In this intercomparison, the $MAPCO_2$ was within 1 µatm compared to the underway pCO_2 reference system in conditions within the calibration gas range.

In summary, the $MAPCO_2$ system performs very well in laboratory and field settings in comparison to a variety of other methods. Considering the precision estimate of the $MAPCO_2$ measurements in the field ($< \pm 0.7$ µmol mol^{-1}), the statistically strong ($p < 0.05$) mean differences in $MAPCO_2$ versus comparison measurements in Table 5 ($< \pm 1.8$ µatm), and the small propagation of error resulting from the xCO_2 (dry) calculation ($< \pm 0.1$ µmol mol^{-1}), we estimate in situ $MAPCO_2$ precision at $< \pm 0.7$ µmol mol^{-1} and accuracy at $< \pm 2.0$ µmol mol^{-1} for xCO_2 (dry) measurements. Overall uncertainty of pCO_2 and fCO_2 observations from the $MAPCO_2$ system is estimated to be < 2.0 µatm for values between 100 and 600 µatm for over 400 days of autonomous operation. However, the uncertainty of finalized, quality-controlled data is likely better for atmospheric pCO_2 and fCO_2 observations at < 1.0 µatm when following the post-deployment standard operating procedures described in Sect. 2.2.

3 Data description and access

Finalized $MAPCO_2$ data are reported to the Carbon Dioxide Information Analysis Center (CDIAC; http://cdiac.ornl.gov/oceans/Moorings) and archived at additional data centers such as the National Oceanographic Data Center (http://www.nodc.noaa.gov). The archived data are organized by site and deployment date. The numeric data package (NDP) associated with this publication includes the 56 deployments listed in Table 6 and is available at doi:10.3334/CDIAC/OTG.TSM_NDP092 or http://cdiac.ornl.gov/oceans/Moorings/ndp092. The methods described here are associated with the mooring pCO_2 data included in this NDP. These data are made freely available to the public and the scientific community in the belief that their wide dissemination will lead to greater understanding and new scientific insights. Users of the data are requested to cite this publication when using the entire open-ocean mooring data set or cite according to the CDIAC data archive when using individual mooring data sets. When preparing manuscripts using these data, users are asked to invite lead pCO_2 mooring investigators to coauthor or to send draft manuscripts using these data to the lead investigators to ensure that the quality and limitations of the data are accurately represented.

The mooring data set includes 3-hourly seawater and atmospheric CO_2 observations from 14 moorings since 2004, encompassing over 100 000 individual measurements. As presented in Fig. 3, climatological means of surface ocean pCO_2 measured on moorings are consistent with observations from other platforms (Bakker et al., 2014; Takahashi et al., 2009); however, much of the value in high-frequency mooring observations is demonstrated at shorter timescales. Figure 3 shows that short-term (≤ 2 years) variability at the subtropical sites tends to be dominated by the seasonal cycle, and tropical sites tend to be dominated by interannual variability. At the subtropical sites, seawater CO_2 is typically highest in the summer and lowest in the winter. The Papa site is the highest-latitude mooring in this data set and exhibits approximately equal short-term variation driven by the seasonal cycle and interannual variability caused by strong weather events in this region of the North Pacific. The highest interannual variability is observed in the equatorial Pacific driven by El Niño and La Niña events (Fig. 3) and dominates any small seasonal signal that may exist in this region (Sutton et al., 2014). In the most extreme conditions, seawater pCO_2 values can vary over 100 µatm within 24 h at 0°, 125° W (Fig. 6a). Variability of 100–150 µatm is also common in the equatorial Pacific during the extension of the warm water pool during El Niño events on timescales of months and the passing of tropical instability waves on timescales of weeks (e.g., Fig. 4 in Sutton et al., 2014). Sustained, long-term mooring time series also provide the opportunity to identify and remove the short-term variability from the time series and investigate long-term trends. For example, in a synthesis of equatorial Pacific mooring data, Sutton et al. (2014) found that the uptake of anthropogenic CO_2 and an acceleration in equatorial upwelling since the shift in the Pacific Decadal Oscillation in 1998 has led to high rates of pCO_2 change of $+2.3$ to $+3.3$ µatm yr^{-1} in this region. This decadal shift in CO_2 outgassing is consistent with underway pCO_2 observations made in this region since 1982 (Feely et al., 2014).

Mooring data from most of the deployments through 2010 listed in Table 6 are also included in the most recent version of SOCAT (Bakker et al., 2014). This SOCATv2.0 synthesis involves a standardized, second-level quality control of 10.1 million surface seawater fCO_2 measurements from many different sources, including underway and mooring

Table 6. List of open-ocean mooring deployments in the open-ocean $MAPCO_2$ data set. n is the total number of measurements collected at each mooring location during these deployments.

Mooring	Start date MM/DD/YYYY	End date MM/DD/YYYY	Mooring	Start date MM/DD/YYYY	End date MM/DD/YYYY
MOSEAN/WHOTS	12/19/2004	05/23/2005	TAO110W	09/19/2009	11/03/2009
	05/29/2005	01/20/2006		03/15/2010	07/14/2010
	06/18/2006	12/21/2006		07/22/2010	10/28/2010
	01/28/2007	07/30/2007	n	2148	
	06/26/2007	06/05/2008			
	06/05/2008	02/12/2009	TAO125W	05/08/2004	12/20/2004
	07/11/2009	08/01/2010		03/16/2005	09/15/2005
	08/01/2010	07/13/2011		01/31/2006	07/08/2006
n	17 645			04/13/2007	07/17/2007
				10/16/2007	11/10/2008
BTM	10/02/2005	07/03/2006		11/13/2008	10/21/2009
	07/14/2006	03/02/2007		04/22/2010	11/06/2010
	03/13/2007	10/01/2007	n	13 609	
n	5354				
			TAO140W	05/23/2004	09/12/2004
Papa	06/08/2007	06/10/2008		09/13/2004	03/01/2005
	06/11/2008	11/11/2008		03/02/2005	09/22/2005
	06/13/2009	03/27/2010		01/17/2006	05/14/2006
	06/16/2010	06/13/2011		09/14/2006	12/18/2006
n	9235			05/31/2007	11/20/2007
				05/10/2008	09/03/2009
KEO	09/28/2007	08/08/2008		09/04/2009	01/30/2010
	09/13/2008	09/04/2009		11/26/2010	03/23/2011
	09/05/2009	09/24/2010	n	14 276	
	09/30/2010	12/24/2010			
n	9182		TAO155W	01/13/2010	08/25/2010
			n	1791	
JKEO	02/18/2007	10/03/2007			
n	1837		TAO170W	07/04/2005	06/23/2006
				07/31/2007	08/13/2008
CCE1	11/11/2008	02/06/2009		08/26/2008	06/01/2009
	05/19/2009	12/14/2009		06/02/2009	12/12/2009
	12/15/2009	09/01/2010		02/03/2010	02/04/2011
	09/02/2010	10/11/2010	n	12 528	
n	4775				
			TAO165E	02/23/2010	02/27/2011
Stratus	10/16/2006	10/29/2007	n	2955	
	10/27/2007	10/27/2008			
	10/26/2008	01/18/2010	TAO8S165E	06/22/2009	09/19/2010
	01/19/2010	07/07/2010		10/18/2010	11/15/2011
n	10 889		n	6720	

systems. SOCAT also produces a gridded surface ocean fCO_2 data product in a uniform format available at http://www.socat.info. Rödenbeck et al. (2013) compared the previous version of SOCAT (v1.5), which did not include mooring data, to some of the open-ocean $MAPCO_2$ time series in Table 6. In a comparison between seawater pCO_2 data from the TAO170W $MAPCO_2$ and data-driven model estimates based on SOCATv1.5, Rödenbeck et al. (2013) find that seawater pCO_2 estimates in the tropics are unrelated, or even opposite, to the mooring observations. This discrepancy arises because that particular location is not well constrained by the SOCATv1.5 data set. We expect the recent mooring additions to SOCATv2.0 and the open-ocean $MAPCO_2$ data set presented here to make a large impact on our efforts to model and understand the global carbon cycle in the coming years.

4 Conclusion

Mooring observations can play a critical role in improving our ability to model, understand, and describe the ocean carbon cycle on all timescales. In particular, time series from remote, data-sparse areas of the ocean collected on moorings fulfill a unique niche by providing the high-resolution data necessary to explore questions about short-term variability at fixed locations. Here we provide a data set of 3-hourly surface seawater and marine boundary layer atmospheric pCO_2 observations on 14 open-ocean moorings in the Pacific and Atlantic from 2004 to 2011. When using the in situ and post-calibration methods described here, overall uncertainty for the $MAPCO_2$ data is < 2 µatm for seawater pCO_2 and < 1 µatm for air pCO_2, making the $MAPCO_2$ system a climate-quality method for tracking surface ocean pCO_2. These types of sustained, temporally resolved observations allow us to improve our understanding of the role of shorter-term variability and key biogeochemical processes on the global carbon system. Potential uses of these data to inform our understanding of a changing ocean include investigating high-frequency variability in surface ocean biogeochemistry, developing seasonal CO_2 flux maps for the global oceans (e.g., Takahashi climatology and SOCAT), studying ocean acidification, and evaluating regional and global carbon models.

Acknowledgements. This work was funded by the Climate Observation Division within NOAA's Climate Program Office. The authors thank Gernot Friederich, Peter Brewer, and Francisco Chavez at the Monterey Bay Aquarium Research Institute for their efforts in developing the early mooring pCO_2 system, and the Battelle Memorial Institute for their later investments in this technology that have made the $MAPCO_2$ systems available to the broader research and ocean-observing community. The NOAA network of pCO_2 moorings would not be possible without the industrious efforts of PMEL technical and engineering staff as well as our partners and their funders who support the maintenance of the open-ocean buoys: Nick Bates (BTM), Meghan Cronin (Papa and KEO), Michael McPhaden (TAO array), Tommy Dickey (MOSEAN), Al Plueddemann and Robert Weller (WHOTS and Stratus), and Uwe Send (CCE1). PMEL contribution 4061 and JISAO contribution 2254.

Edited by: D. Carlson

References

Bakker, D. C. E., Pfeil, B., Smith, K., Hankin, S., Olsen, A., Alin, S. R., Cosca, C., Harasawa, S., Kozyr, A., Nojiri, Y., O'Brien, K. M., Schuster, U., Telszewski, M., Tilbrook, B., Wada, C., Akl, J., Barbero, L., Bates, N. R., Boutin, J., Bozec, Y., Cai, W.-J., Castle, R. D., Chavez, F. P., Chen, L., Chierici, M., Currie, K., de Baar, H. J. W., Evans, W., Feely, R. A., Fransson, A., Gao, Z., Hales, B., Hardman-Mountford, N. J., Hoppema, M., Huang, W.-J., Hunt, C. W., Huss, B., Ichikawa, T., Johannessen, T., Jones, E. M., Jones, S. D., Jutterström, S., Kitidis, V., Körtzinger, A., Landschützer, P., Lauvset, S. K., Lefèvre, N., Manke, A. B., Mathis, J. T., Merlivat, L., Metzl, N., Murata, A., Newberger, T., Omar, A. M., Ono, T., Park, G.-H., Paterson, K., Pierrot, D., Ríos, A. F., Sabine, C. L., Saito, S., Salisbury, J., Sarma, V. V. S. S., Schlitzer, R., Sieger, R., Skjelvan, I., Steinhoff, T., Sullivan, K. F., Sun, H., Sutton, A. J., Suzuki, T., Sweeney, C., Takahashi, T., Tjiputra, J., Tsurushima, N., van Heuven, S. M. A. C., Vandemark, D., Vlahos, P., Wallace, D. W. R., Wanninkhof, R., and Watson, A. J.: An update to the Surface Ocean CO_2 Atlas (SOCAT version 2), Earth Syst. Sci. Data, 6, 69–90, doi:10.5194/essd-6-69-2014, 2014.

Bender, M., Doney, S., Feely, R. A., Fung, I. Y., Gruber, N., Harrison, D. E., Keeling, R., Moore, J., Sarmiento, J., Sarachik, E., Stephens, B., Takahashi, T., Tans, P. P., and Wanninkhof, R.: A Large Scale Carbon Observing Plan: In Situ Oceans and Atmosphere (LSCOP), Nat. Tech. Info. Service, Springfield, 201 pp., 2002.

Buck, A. L.: New equations for computing vapor pressure and enhancement factor, J. Appl. Meteorol., 20, 1527–1532, 1981.

Feely, R. A., Wanninkhof, R., Milburn, H. B., Cosca, C. E., Stapp, M., and Murphy, P.: A new automated underway system for making high precision pCO_2 measurements onboard research ships, Anal. Chim. Acta, 377, 185–191, doi:10.1016/S0003-2670(98)00388-2, 1998.

Feely, R. A., Cosca, C. E., Sutton, A. J., Sabine, C. L., Wanninkhof, R., and Mathis, J. T.: Decadal changes of air-sea CO_2 fluxes in the Equatorial Pacific Ocean, Geophys. Res. Lett., in preparation, 2014.

Friederich, G. E., Brewer, P. G., Herlien, R., and Chavez, F. P.: Measurement of sea surface partial pressure of CO_2 from a moored buoy, Deep-Sea Res. Pt. I, 42, 1175–1186, doi:10.1016/0967-0637(95)00044-7, 1995.

GLOBALVIEW-CO2: Cooperative Global Atmospheric Data Integration Project, 2013, updated annually, Multi-laboratory compilation of synchronized and gap-filled atmospheric carbon dioxide records for the period 1979–2012 (obspack_co2_1_GLOBALVIEW-CO2_2013_v1.0.4_2013-12-23), compiled by NOAA Global Monitoring Division: Boulder, Colorado, USA Data product accessed at: doi:10.3334/OBSPACK/1002, 2013.

Hofmann, D. J., Butler, J. H., and Tans, P. P.: A new look at atmospheric carbon dioxide, Atmos. Environ., 43, 2084–2086, doi:10.1016/j.atmosenv.2008.12.028, 2009.

Keeling, C. D., Bacastow, R. B., Bainbridge, A. E., Ekdahl, C. A., Guenther, P. R., Waterman, L. S., and Chin, J. F. S.: Atmospheric carbon dioxide variations at Mauna Loa Observatory, Hawaii, Tellus, 28, 538–551, doi:10.1111/j.2153-3490.1976.tb00701.x, 1976.

Lewis, E. and Wallace, D. W. R.: Program Developed for CO2 System Calculations, Carbon Dioxide Information Analysis Center, Oak Ridge National Laboratory, U.S. Department of Energy, Oak Ridge, Tennessee, 1998.

Lueker, T. J., Dickson, A. G., and Keeling, C. D.: Ocean pCO_2 calculated from dissolved inorganic carbon, alkalinity, and equations for K1 and K2: validation based on laboratory measurements of CO_2 in gas and seawater at equilibrium, Mar. Chem., 70, 105–119, doi:10.1016/S0304-4203(00)00022-0, 2000.

Pfeil, B., Olsen, A., Bakker, D. C. E., Hankin, S., Koyuk, H., Kozyr, A., Malczyk, J., Manke, A., Metzl, N., Sabine, C. L., Akl, J., Alin, S. R., Bates, N., Bellerby, R. G. J., Borges, A., Boutin, J., Brown, P. J., Cai, W.-J., Chavez, F. P., Chen, A., Cosca, C., Fassbender, A. J., Feely, R. A., González-Dávila, M., Goyet, C., Hales, B., Hardman-Mountford, N., Heinze, C., Hood, M., Hoppema, M., Hunt, C. W., Hydes, D., Ishii, M., Johannessen, T., Jones, S. D., Key, R. M., Körtzinger, A., Landschützer, P., Lauvset, S. K., Lefèvre, N., Lenton, A., Lourantou, A., Merlivat, L., Midorikawa, T., Mintrop, L., Miyazaki, C., Murata, A., Nakadate, A., Nakano, Y., Nakaoka, S., Nojiri, Y., Omar, A. M., Padin, X. A., Park, G.-H., Paterson, K., Perez, F. F., Pierrot, D., Poisson, A., Ríos, A. F., Santana-Casiano, J. M., Salisbury, J., Sarma, V. V. S. S., Schlitzer, R., Schneider, B., Schuster, U., Sieger, R., Skjelvan, I., Steinhoff, T., Suzuki, T., Takahashi, T., Tedesco, K., Telszewski, M., Thomas, H., Tilbrook, B., Tjiputra, J., Vandemark, D., Veness, T., Wanninkhof, R., Watson, A. J., Weiss, R., Wong, C. S., and Yoshikawa-Inoue, H.: A uniform, quality controlled Surface Ocean CO_2 Atlas (SOCAT), Earth Syst. Sci. Data, 5, 125–143, doi:10.5194/essd-5-125-2013, 2013.

Pierrot, D., Neill, C., Sullivan, K., Castle, R., Wanninkhof, R., Lüger, H., Johannessen, T., Olsen, A., Feely, R. A., and Cosca, C. E.: Recommendations for autonomous underway pCO_2 measuring systems and data-reduction routines, Deep-Sea Res. Pt. II, 56, 512–522, doi:10.1016/j.dsr2.2008.12.005, 2009.

Rödenbeck, C., Keeling, R. F., Bakker, D. C. E., Metzl, N., Olsen, A., Sabine, C., and Heimann, M.: Global surface-ocean pCO_2 and sea–air CO_2 flux variability from an observation-driven ocean mixed-layer scheme, Ocean Sci., 9, 193-216, doi:10.5194/os-9-193-2013, 2013.

Sabine, C., Ducklow, H., and Hood, M.: International carbon coordination: Roger Revelle's legacy in the Intergovernmental Oceanographic Commission, Oceanography, 23, 48–61, 2010.

Schar, D., Atkinson, M., Johengen, T., Pinchuk, A., Purcell, H., Robertson, C., Smith, G. J., and Tamburri, M.: Performance demonstration statement PMEL MAPCO$_2$/Battelle Seaology pCO_2 Monitoring System, UMCES Technical Report Series: Ref. No. [UMCES]CBL 10-092, 2010.

Sutton, A. J., Feely, R. A., Sabine, C. L., McPhaden, M. J., Takahashi, T., Chavez, F. P., Friederich, G. E., and Mathis, J. T.: Natural variability and anthropogenic change in equatorial Pacific surface ocean pCO_2 and pH, Global Biogeochem. Cy., 2013, GB004679, doi:10.1002/2013gb004679, 2014.

Takahashi, T.: Carbon dioxide in the atmosphere and in Atlantic Ocean water, J. Geophys. Res., 66, 477–494, 1961.

Takahashi, T., Sutherland, S. C., Wanninkhof, R., Sweeney, C., Feely, R. A., Chipman, D. W., Hales, B., Friederich, G., Chavez, F., Sabine, C., Watson, A., Bakker, D. C. E., Schuster, U., Metzl, N., Yoshikawa-Inoue, H., Ishii, M., Midorikawa, T., Nojiri, Y., Körtzinger, A., Steinhoff, T., Hoppema, M., Olafsson, J., Arnarson, T. S., Tilbrook, B., Johannessen, T., Olsen, A., Bellerby, R., Wong, C. S., Delille, B., Bates, N. R., and de Baar, H. J. W.: Climatological mean and decadal change in surface ocean pCO_2, and net sea-air CO_2 flux over the global oceans, Deep-Sea Res. Pt. II, 56, 554–577, doi:10.1016/j.dsr2.2008.12.009, 2009.

Thoning, K. W., Tans, P. P., and Komhyr, W. D.: Atmospheric carbon dioxide at Mauna Loa Observatory: 2. Analysis of the NOAA GMCC data, 1974–1985, J. Geophys. Res.-Atmos., 94, 8549–8565, doi:10.1029/JD094iD06p08549, 1989.

UNESCO: SOCAT Equatorial Pacific, North Pacific, and Indian Ocean Regional Workshop, Tokyo, Japan, 8–11 February 2010, IOC Workshop Report No. 229, available at: http://www.ioccp.org/images/D3meetingReports/WR229_eo.pdf (last access: 29 October 2014), 2010.

Wanninkhof, R. and Thoning, K.: Measurement of fugacity of carbon dioxide in surface water and air using continuous sampling methods, Mar. Chem., 44, 189–205, 1993.

Wanninkhof, R., Park, G.-H., Takahashi, T., Sweeney, C., Feely, R., Nojiri, Y., Gruber, N., Doney, S. C., McKinley, G. A., Lenton, A., Le Quéré, C., Heinze, C., Schwinger, J., Graven, H., and Khatiwala, S.: Global ocean carbon uptake: magnitude, variability and trends, Biogeosciences, 10, 1983–2000, doi:10.5194/bg-10-1983-2013, 2013.

Weiss, R. F.: Carbon dioxide in water and seawater: the solubility of a non-ideal gas, Mar. Chem., 2, 203–215, doi:10.1016/0304-4203(74)90015-2, 1974.

Weiss, R. F. and Price, B. A.: Nitrous oxide solubility in water and seawater, Mar. Chem., 8, 347–359, doi:10.1016/0304-4203(80)90024-9, 1980.

Weiss, R. F., Jahnke, R. A., and Keeling, C. D.: Seasonal effects of temperature and salinity on the partial pressure of CO_2 in seawater, Nature, 300, 511–513, 1982.